MuSun - Muon Capture on the Deuteron

P. Kammel[1⋆] on behalf of the MuSun collaboration[1]

1 Center for Experimental Nuclear Physics and Astrophysics, and Department of Physics, University of Washington, Seattle, WA 98195, USA
* pkammel@uw.edu

February 10, 2021

Review of Particle Physics at PSI
doi:10.21468/SciPostPhysProc.2

Abstract

The MuSun experiment is a precision measurement of the rate for nuclear muon capture on the deuteron, designed to resolve a long-standing disagreement between experiment and theory, and to determine an important low-energy constant relevant for a variety of weak and strong dynamics. The experiment is based on a novel active target method employing a pure deuterium cryogenic time-projection chamber. The data taking was completed in two main campaigns and the analysis is well advanced. The unique challenges and corresponding strategy of the experiment as well as the status of the analysis are presented.

18.1 Introduction

Muon capture is a powerful tool to study the properties and structure of the nucleon and few nucleon systems as predicted by effective theories (EFT) founded on Quantum Chromodynamics. Our program focuses on capture from the simplest of all muonic atoms, namely on the proton in the theoretically-pristine muonic hydrogen (MuCap experiment) [1–3] as well as on the simplest nucleus in muonic deuterium (MuSun experiment [4]), which is presented here. Our collaboration has pioneered a novel active-target method based upon the development of high-pressure time-projection chambers (TPC) filled with hydrogen/deuterium gas, and in an earlier experiment ^{3}He [5].

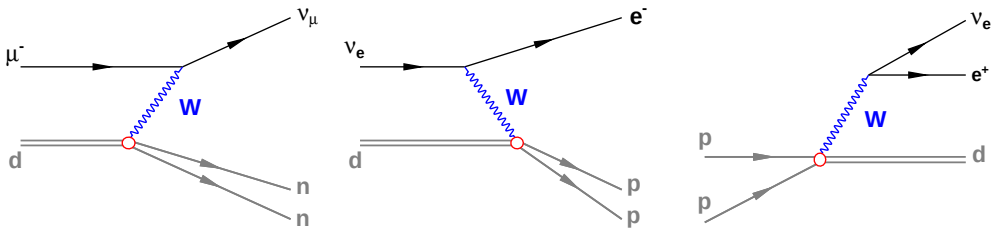

Figure 18.1: The hadronic vertex (red circle) in the three weak processes muon capture, neutrino deuteron scattering and pp fusion is characterized by a common parameter.

[1]Petersburg Nuclear Physics Inst. - Univ. of Washington - Paul Scherrer Inst. - Univ. of Kentucky - Boston Univ. - Univ. Cath. Louvain - Regis Univ. - Univ. of South Carolina

One of the most interesting topics for muon capture in the few-body sector is the family of two-nucleon weak-interaction processes. As shown in Figure 18.1 this family contains muon capture on the deuteron,

$$\mu + d \rightarrow n + n + \nu \tag{18.1}$$

together with two astrophysics reactions of fundamental interest, in particular, pp fusion, which is the primary energy source in the sun and the main sequence stars, and the νd reactions, which provides the evidence for solar neutrino oscillations by measuring the flavor-separated neutrino flux at the Sudbury Neutrino Observatory. The extremely small rates of these processes do not allow their cross sections to be measured under terrestrial conditions; they can only be calculated by theory [6–9], with information derived from the more-complex three-nucleon system.

These interactions all involve the same axial-vector coupling at a four-nucleon vertex [10, 11], the two-nucleon analog to g_A for the nucleon. The strength of this coupling is characterized by a single, poorly known low energy constant (LEC) in the EFT description up to the required order. Moreover, this LEC is an essential ingredient in the construction of chiral three-nucleon forces [12, 13] and in other weak and strong processes [14, 15].

MuSun plans to determine the rate Λ_d of muon capture on the deuteron to 1.5%, where Λ_d denotes the capture rate from the doublet hyperfine state in a muonic deuterium atom. Current experiments are at the 6-10% level, and the most precise one [16] disagrees with the latest theory calculation of $\Lambda_d = 399 \pm 3\,\mathrm{s}^{-1}$ [8, 9], see also [17], by more than 3-sigma. The LEC will be determined at the 20% level, i.e. 5 times better than what is presently known from the two-nucleon system.

18.2 MuSun Experiment

The MuSun experiment uses the so-called “lifetime method" consisting of a precision measurement of the muon disappearance rate in deuterium. The time distribution of electrons from muon decay in deuterium follows[2]

$$\frac{dN_e}{dt}(t) \propto e^{-(\lambda_{\mu^+} + \Lambda_d)\,t} \tag{18.2}$$

i.e. the disappearance rate $\lambda_{d\mu}$ measured by MuSun is the sum of the free muon decay rate λ_{μ^+} [18], and the capture rate Λ_d. Λ_d is determined by subtracting the precisely known λ_{μ^+} from $\lambda_{d\mu}$. The basic experimental technique is similar to the MuCap experiment described in Section 17 [3]. Muons pass through the entrance detectors and a beryllium window to stop in a cryogenic time-projecton-chamber (cryo-TPC) filled with ultra-pure deuterium gas (Figure 18.2). Decay electrons are detected in two cylindrical wire chambers and a 16-fold segmented scintillator barrel. The lifetime is determined from the measured time difference between the fast muon entrance detector and the decay electron scintillator array. After a muon hits the entrance counter, a fast kicker [19] turns off the beam for the measurement interval to reduce pileup.

The experiment must simultaneously meet several stringent requirements. i) The target conditions (T=31 K and density 6.5% of liquid-hydrogen density) are optimized for an unambiguous extraction of Λ_d, and the suppression of muonic atomic-physics complications that arise when muons stop in deuterium, such as muon-catalyzed fusion [20]. ii) Muons are stopped in an active target, the unique high-density cyro-TPC, specifically developed for MuSun. Three-dimensional tracking in the TPC eliminates most muon-stops in wall material. High-Z material is used for most TPC materials, so that remaining muons stopping there are

[2] approximate expression after muons have reached the doublet hyperfine state.

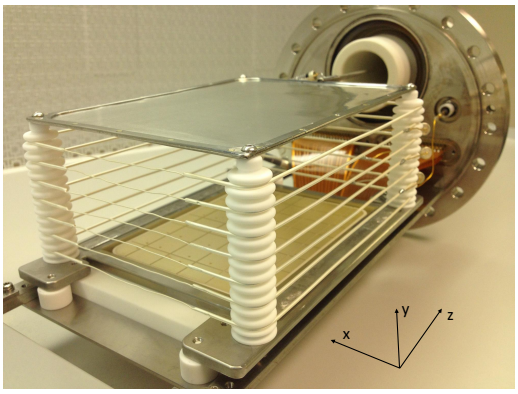

Figure 18.2: Cryogenic TPC with a sensitive volume of 9.6×7.1×12.5 cm^3 segmented into 6×8 pads. Muon beam enters from the front. The grid and field cage wires are made of gold and silver plated tungsten, respectively, and the HV anode consists of a silver foil. The grid frame has a composite construction to withstand thermal cycling.

quickly captured. iii) Muon transfer to impurity elements, where capture occurs with a much higher rate than in deuterium, is suppressed by keeping the gas contamination at the 10^{-9} level with a continuous circulation and filter system [21]. The purity is monitored *in situ* in the TPC by gas chromatography [22]. Isotopically pure deuterium was produced in an on-site cryogenic distillation system [23].

The high gas density in the cryo-TPC requires a drift voltage of 80 kV to achieve a drift velocity of 5 mm/μs and prohibits signal amplification in the gas. Thus the TPC was operated as an ionization chamber. A challenging aspect of the design was the Frisch grid, which was strung with gold-plated tungsten wires of 50 μm diameter with 400 μm pitch. It features a composite frame, where the side bars along the wires direction were also made of tungsten to match the thermal expansion while the cross bars were made of stainless steel to allow soldering the wires. This construction withstood numerous cryogenic temperature cycles over several years without damage. Excellent energy resolution of ≈17 keV rms was realized with custom built cyro-preamplifiers [24] which operated inside the insulation vacuum in close vicinity to the TPC at a stabilized temperature of 140 K.

After several technical developments and upgrades, MuSun collected its full statistics of 1.4×10^{10} events in two main production runs R2014 and R2015 at the PSI πE1 beamline, followed, in 2016, by a shorter run focused on systematic effects.

18.3 Status of the Analysis

As the capture rate Λ_d amounts to less than one per mill of the muon decay rate λ_{μ^+}, the muon disappearance rate $\lambda_{d\mu}$ has to be measured to 13 ppm to determine Λ_d to 1.5% or $\pm$ 6 s^{-1}. Such a precision requires careful attention to systematics from physical as well as instrumental effects. In particular early to late effects within the fit range of 1-24 μs must be tightly controlled.

The analysis starts with the muon stop definition. This is a critical step as subsequent muon-catalyzed-fusion products can overlap the muon track, see Figure 18.3, leading to mis-reconstruction of the muon stopping point. Most tracks are muon stops with energy deposition up to 1.5 MeV. However, $d\mu$ atoms can combine to muonic $dd\mu$ molecules, from which spontaneous fusion proceeds in two branches ^{3}He (0.8 MeV)+n (2.4 MeV) and p (3.0 MeV)+t (1.0 MeV). The higher energy structures in the μ^- spectrum are indicative for fusion recoils not separated from the muon tracks. While the time distribution of all decays is well described by (18.2), the time distributions for decay electrons with or without fusion reactions differ. Thus

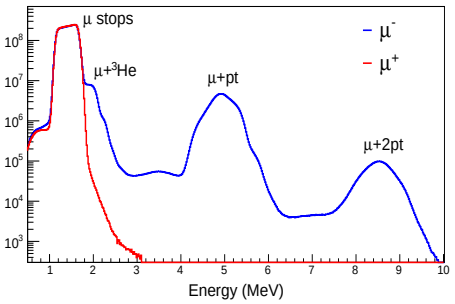

Figure 18.3: Energy deposition in TPC around muon stop location. Pileup with fusion recoils from ^{3}He and pt leads to distinct structures at higher energies in the μ^- spectrum. The μ^+ spectrum with lower statistics was scaled up.

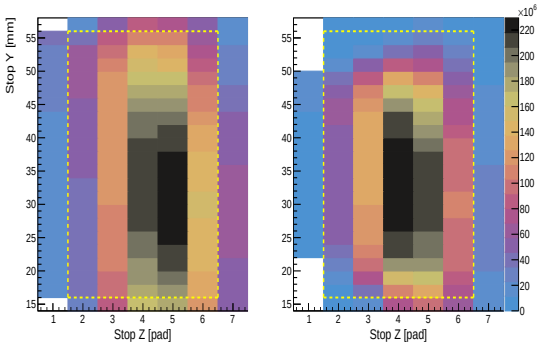

Figure 18.4: Muon stopping distribution in y-z projection with fiducial boundaries (yellow lines). The full stopping distribution (left panel) can be shaped by cuts on the first TPC pad row to reduce the muon population close to the boundaries (right panel).

both event types have to be reconstructed with the same acceptance at sub percent accuracy to avoid biasing the lifetime measurement. The dominant mechanism for acceptance differences are misreconstruction of muon stops at the TPC fiducial boundaries caused by the overlap with the 3 MeV protons from p+t reactions which have a range of 13 mm. The approach to study these corrections is indicated in Figure 18.4. By imposing x, y and dE/dx cuts on the first pad row of the TPC the stopping distribution can be shaped in all dimensions, reducing or enhancing the muon population at the fiducial volume boundaries and quantifying the associated acceptance losses. Currently the uncertainty of this method is estimated as $\approx 6\,\mathrm{s}^{-1}$.

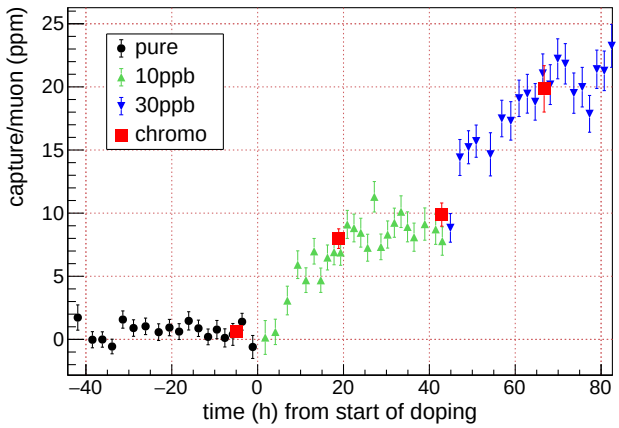

Figure 18.5: Calibration of capture yield from N_2 impurities. After an initial high purity run, the circulating flow was doped with 10 ppb and 30 ppb admixtures, respectively. The concentrations build up over hours in the TPC as monitored by the increasing yield of capture recoils. The chromatography measurements (red squares) track the capture yield and are used to calibrate it.

At the operating temperature T=31 K of MuSun, most impurities have frozen out, but the partial pressure of potential nitrogen trace admixtures would be too high. As the rate for muon transfer from deuterium to nitrogen at cryogenic conditions was unknown, MuSun determined

the sensitivity to the nitrogen concentration c_N in a dedicated experiment as $\partial\lambda_{d\mu}/\partial c_N \approx 4\,\mathrm{s}^{-1}$ per ppb. During R2015 the MuSun chromatography was able to limit c_N to about 1 ppb [22]. A more direct method applied to all runs is the detection of the capture recoil from $\mu+N \rightarrow C^*+\nu$ in the TPC, c.f. Figure 18.5. Identifying those rare low energy signals of about 150 keV is challenging against the background of Michel electrons and ^{3}He recoils, but was achieved due to the excellent energy resolution of the cryo-TPC. This analysis is in progress, as the observed capture yield still requires a correction for scattering of $\mu+d$ capture neutrons inside the TPC.

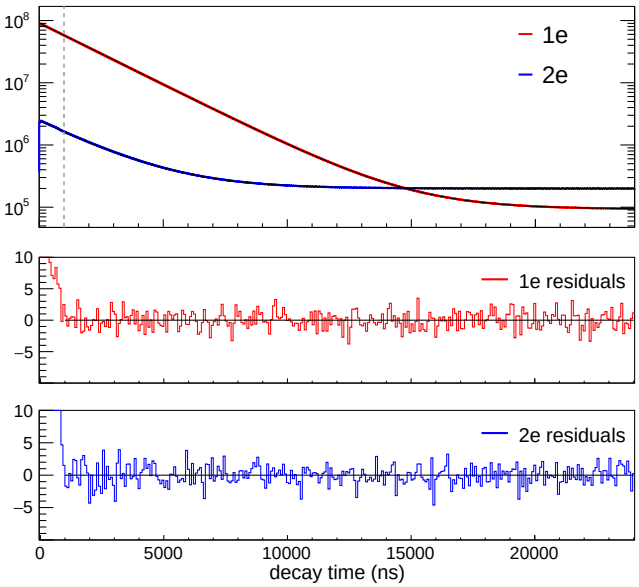

Figure 18.6: Muon decay spectra from scintillators observed in R2014 requiring one (1e) or two (2e) electrons in the region of interest of 0-24000 ns. The fit range is 1-24 μs with a bin width of 40 ns. The fit model is a single exponential and an accidental component with a small linear term. The fit curves and the data are not discernible by eye. The normalized residual plots demonstrate consistency once early kicker induced background has subsided.

The muon decay spectra, see Figure 18.6, are built by histogramming the electron scintillator barrel hits against the entrance scintillator time for muons that were tracked to stop inside the fiducial volume of the TPC. For decay electrons the signals in the scintillator are used or, alternatively, this information is combined with tracking in the electron wire chambers. This provides some complementarity, as the scintillators are fast and simple, while the chambers are slower and more sensitive to noise pickup but define an electron track vector. The time spectra shown in the figure are sorted depending whether only one (1e), or two (2e) electrons were detected in the region of interest (ROI) 0-24 μs after muons stop. In the 1e spectrum accidentals are suppressed as their detection probability is decreased by (1 - ϵ_e), where $\epsilon_e = 0.7$ is the detection efficiency for Michel electrons. On the other hand, in the 2e spectrum muon decay electrons are suppressed by the small probability of $\approx 3\%$ of an accidental hit within the ROI. Thus the 1e time spectrum is favorable to obtain clean decay information, while the 2e spectrum is useful to study the properties of the background. In fact, a slight time-dependent decrease of the background is observed, which is probably related to the fast kicker, and is accounted for in a simultaneous fit of both spectra. The linear correction term leads to a few Hz shift in the fitted disappearance rate $\lambda_{\mu d}$ with an uncertainty currently estimated as $\approx 3\,\mathrm{s}^{-1}$.

A fraction of the data has been taken with a μ^+ beam to study systematic effects free of the aforementioned μ^- physics processes, albeit with the additional complication of muon spin rotation affecting positive muons. This data has been unblinded and found in agreement

with the MuLan muon lifetime [18] (see also Section 16 [25]), well within the statistical uncertainty of 21 s^{-1} of the MuSun μ^+ dataset. This is an important consistency check to limit instrumental systematic effects that apply to μ^- as well to μ^+.

18.4 Summary and Outlook

The strategy and analysis of the MuSun experiment has been described. In particular, the main sources of uncertainty have been discussed, while deferring several others to a more detailed publication. The presence of muon-catalyzed-fusion in deuterium, absent in MuCap, required intricate studies of the cryo-TPC response derived from high statistics datasets. The analysis is advanced with final work and cross checks still under way. The collaboration plans to unblind the first μ^- dataset R2014 within the next few months, which has sufficient statistics to clarify the long-standing discrepancy between experiment and theory on nuclear muon capture on the deuteron. The final analysis will include a larger second dataset R2015 to obtain a capture rate with 1-2% uncertainty, commensurate with the current precision of theoretical calculations. The comparison of experiment and theory will test whether there are still surprises in the description of the weak coupling of the two-nucleon system and will establish a low-energy constant relevant for a variety of weak and strong dynamics.

Acknowledgment

The work was supported by the US Department of Energy Office of Science, Office of Nuclear Physics under Award No. DE-FG02-97ER41020, and used the Extreme Science and Engineering Discovery Environment (XSEDE), which is supported by National Science Foundation grant number ACI-1548562.

References

[1] V. A. Andreev, T. I. Banks, R. M. Carey, T. A. Case, S. M. Clayton, K. M. Crowe, J. Deutsch, J. Egger, S. J. Freedman, V. A. Ganzha, T. Gorringe, F. E. Gray *et al.*, *Measurement of muon capture on the proton to 1determination of the pseudoscalar coupling g_P*, Phys. Rev. Lett. **110**, 012504 (2013), doi:10.1103/PhysRevLett.110.012504.

[2] V. A. Andreev, T. I. Banks, R. M. Carey, T. A. Case, S. M. Clayton, K. M. Crowe, J. Deutsch, J. Egger, S. J. Freedman, V. A. Ganzha, T. Gorringe, F. E. Gray *et al.*, *Measurement of the formation rate of muonic hydrogen molecules*, Phys. Rev. C **91**, 055502 (2015), doi:10.1103/PhysRevC.91.055502.

[3] M. Hildebrandt and C. Petitjean, *MuCap: Muon Capture on the Proton*, SciPost Phys. Proc. **2**, ppp (2021), doi:10.21468/SciPostPhysProc.2.XXX.

[4] V. A. Andreev *et al.*, *Muon Capture on the Deuteron – The MuSun Experiment* (2010), 1004.1754.

[5] P. Ackerbauer *et al.*, *A precision measurement of nuclear muon capture on He-3*, Phys. Lett. **B417**, 224 (1998), doi:10.1016/S0370-2693(97)01382-8, hep-ph/9708487.

[6] E. G. Adelberger, A. García, R. H. Robertson, K. A. Snover, A. B. Balantekin, K. Heeger, M. J. Ramsey-Musolf, D. Bemmerer, A. Junghans, C. A. Bertulani and others, *Solar fusion cross sections. II. the p p chain and CNO cycles*, Reviews of Modern Physics **83**(1), 195 (2011).

[7] B. Acharya, B. Carlsson, A. Ekström, C. Forssén and L. Platter, *Uncertainty quantification for proton–proton fusion in chiral effective field theory*, Physics Letters B **760**, 584 (2016), doi:10.1016/j.physletb.2016.07.032.

[8] L. Marcucci, A. Kievsky, S. Rosati, R. Schiavilla and M. Viviani, *Chiral effective field theory predictions for muon capture on deuteron and ^{3}He*, Phys. Rev. Lett. **108**, 052502 (2012), doi:10.1103/PhysRevLett.108.052502, 1109.5563.

[9] L. E. Marcucci, A. Kievsky, S. Rosati, R. Schiavilla and M. Viviani, *Erratum: Chiral effective field theory predictions for muon capture on deuteron and ^{3}He [phys. rev. lett. 108, 052502 (2012)]*, Phys. Rev. Lett. **121**, 049901 (2018), doi:10.1103/PhysRevLett.121.049901.

[10] J.-W. Chen, K. M. Heeger and R. G. H. Robertson, *Constraining the leading weak axial two-body current by SNO and super-K*, Phys. Rev. **C67**, 025801 (2003), doi:10.1103/PhysRevC.67.025801, nucl-th/0210073.

[11] S. Pastore, F. Myhrer and K. Kubodera, *An update of muon capture on hydrogen*, Int. J. Mod. Phys. **E23**(08), 1430010 (2014), doi:10.1142/S0218301314300100, 1405.1358.

[12] D. Gazit, S. Quaglioni and P. Navrátil, *Three-nucleon low-energy constants from the consistency of interactions and currents in chiral effective field theory*, Physical Review Letters **103**(10), 102502 (2009), doi:10.1103/PhysRevLett.103.102502.

[13] D. Gazit, S. Quaglioni and P. Navrátil, *Erratum: Three-nucleon low-energy constants from the consistency of interactions and currents in chiral effective field theory [phys. rev. lett. **103** , 102502 (2009)]*, Physical Review Letters **122**(2), 029901 (2019), doi:10.1103/PhysRevLett.122.029901.

[14] G. B. King, L. Andreoli, S. Pastore, M. Piarulli, R. Schiavilla, R. B. Wiringa, J. Carlson and S. Gandolfi, *Chiral effective field theory calculations of weak transitions in light nuclei*, Physical Review C **102**(2), 025501 (2020), doi:10.1103/PhysRevC.102.025501.

[15] T. Hüther, K. Vobig, K. Hebeler, R. Machleidt and R. Roth, *Family of chiral two- plus three-nucleon interactions for accurate nuclear structure studies*, Physics Letters B **808**, 135651 (2020), doi:10.1016/j.physletb.2020.135651.

[16] G. Bardin, J. Duclos, J. Martino, A. Bertin, M. Capponi, M. Piccinini and A. Vitale, *A measurement of the muon capture rate in liquid deuterium by the lifetime technique*, Nuclear Physics A **453**(4), 591 (1986), doi:10.1016/0375-9474(86)90253-8.

[17] B. Acharya, A. Ekström and L. Platter, *Effective-field-theory predictions of the muon-deuteron capture rate*, Physical Review C **98**(6), 065506 (2018), doi:10.1103/PhysRevC.98.065506.

[18] V. Tishchenko, S. Battu, R. M. Carey, D. B. Chitwood, J. Crnkovic, P. T. Debevec, S. Dhamija, W. Earle, A. Gafarov, K. Giovanetti, T. P. Gorringe, F. E. Gray *et al.*, *Detailed report of the mulan measurement of the positive muon lifetime and determination of the fermi constant*, Phys. Rev. D **87**, 052003 (2013), doi:10.1103/PhysRevD.87.052003.

[19] M. J. Barnes and G. D. Wait, *A 25-kv 75-khz kicker for measurement of muon lifetime*, IEEE Trans. Plasma Sci. **32**, 1932 (2004), doi:10.1109/TPS.2004.835455.

[20] P. Kammel and K. Kubodera, *Precision muon capture*, Ann. Rev. Nucl. Part. Sci. **60**, 327 (2010), doi:10.1146/annurev-nucl-100809-131946.

[21] V. Ganzha, P. Kravtsov, O. Maev, G. Schapkin, G. Semenchuk, V. Trofimov, A. Vasilyev, M. Vznuzdaev, S. Clayton, P. Kammel, B. Kiburg, M. Hildebrandt *et al.*, *A circulating hydrogen ultra-high purification system for the mucap experiment*, Nuclear Instruments and Methods in Physics Research Section A: Accelerators, Spectrometers, Detectors and Associated Equipment **578**(3), 485 (2007), doi:https://doi.org/10.1016/j.nima.2007.06.010.

[22] V. Ganzha, K. Ivshin, P. Kammel, P. Kravchenko, P. Kravtsov, C. Petitjean, V. Trofimov, A. Vasilyev, A. Vorobyov, M. Vznuzdaev and F. Wauters, *Measurement of trace impurities in ultra pure hydrogen and deuterium at the parts-per-billion level using gas chromatography*, Nuclear Instruments and Methods in Physics Research Section A: Accelerators, Spectrometers, Detectors and Associated Equipment **880**, 181 (2018), doi:10.1016/j.nima.2017.10.096.

[23] I. Alekseev, E. Arkhipov, S. Bondarenko, O. Fedorchenko, V. Ganzha, K. Ivshin, P. Kammel, P. Kravtsov, C. Petitjean, V. Trofimov, A. Vasilyev, T. Vasyanina *et al.*, *Cryogenic distillation facility for isotopic purification of protium and deuterium*, Review of Scientific Instruments **86**(12), 125102 (2015), doi:10.1063/1.4936413, https://doi.org/10.1063/1.4936413.

[24] R. A. Ryan, F. Wauters, F. E. Gray, P. Kammel, A. Nadtochy, D. Peterson, T. van Wechel, E. Gross, M. Gubanich, L. Kochenda, P. Kravtsov, D. Orozco *et al.*, *Design and operation of a cryogenic charge-integrating preamplifier for the MuSun experiment*, Journal of Instrumentation **9**(07), P07029 (2014), doi:10.1088/1748-0221/9/07/p07029.

[25] R. Carey, T. Gorringe and D. Hertzog, *Mulan: a part-per-million measurement of the muon lifetime and determination of the Fermi constant*, SciPost Phys. Proc. **2**, ppp (2021), doi:10.21468/SciPostPhysProc.2.XXX.